RSC Advances

PAPER

View Article Online
View Journal | View Issue

Cite this: *RSC Adv.*, 2022, **12**, 3180

Preparation of eugenol nanoemulsions for antibacterial activities

Xuan Fu,[ab] Yuan Gao,[ab] Weiyao Yan,[c] Ziluo Zhang,[ab] Shovra Sarker,[ab] Yinyan Yin,[ab] Qi Liu,*[ab] Jianguo Feng*[c] and Jing Chen*[ab]

Eugenol is a versatile plant essential oil, but its high volatility and low water solubility greatly limit its application. Accordingly, this study prepared eugenol nanoemulsions by a high-speed shearing technique. Through visual inspection and a series of characterizations, including dynamic light scattering, and confocal laser scanning microscopy, the optimized formula was determined to be 5% (w/w) oil phase (eugenol) and 8% (w/w) surfactant (Tween-80), and the optimized shearing time was 5 min. The optimized nanoemulsion had good stability, small droplets (85 nm), and uniform distribution. At a concentration of 0.02 mg μL^{-1}, the nanoemulsion showed strong inhibition against *Escherichia coli* (*E. coli*) and *Staphylococcus aureus* (*S. aureus*). Scanning electron microscopy (SEM) images showed severe deformation and membrane rupture of both bacteria treated by the nanoemulsion. This result was further confirmed by the leakage of proteins in both bacteria after treatment. The results of reactive oxygen species (ROS) and malondialdehyde (MDA) measurements indicated that the increased levels of ROS in both bacteria treated by the nanoemulsion triggered lipid peroxidation, thus increasing the MDA levels, ultimately causing changes in cell membrane permeability and disruption of the membrane structure. In addition, the nanoemulsion had a small effect on the proliferation and apoptosis of hepatocytes (L02) and lung cells (BEAS-2B), indicating its good biocompatibility. In this study, we developed a novel eugenol nanoemulsion with high stability and good biological activity, which may provide a promising and effective method for wound treatment in the healthcare area.

Received 8th November 2021
Accepted 12th January 2022

DOI: 10.1039/d1ra08184e

rsc.li/rsc-advances

Introduction

Infectious disease is a permanent global challenge, and it is the third leading cause of death in developed countries.[1,2] Some clinical diseases are associated with bacterial microbial infections. *E. coli* and *S. aureus* are common bacteria in the medical field. Adherent invasive *E. coli* causes highly pathogenic Crohn's disease by infecting the patient's ileum.[3] *S. aureus* can cause many diseases, including sepsis, pneumonia, endocarditis, toxic shock syndrome, and implant-associated biofilm infections.[4] Bacteria can also exacerbate tumor development through an inflammatory response and the secretion of toxins, bacterial enzymes, and oncogenic peptides.[5] For example, *Helicobacter pylori* can induce chronic inflammation, impaired gastric acidification, and changes in cell proliferation and apoptosis, which can contribute to the development of gastric cancer.[6] Here, the important influence of bacteria in the development and progression of cancer has been well confirmed.

The main antimicrobial agents currently used in the medical field are antibiotics, metal particles, and biomaterials. The use of antibiotics, such as β-lactams, cephalosporins or carbapenems, aminoglycosides, and sulfonamides, is highly successful against many bacteria, but the low locus effect, the route of administration, and associated resistance has limited its further use.[7–9] Metal nanoparticles have a wide range of antimicrobial activity because of the oxidative stress caused by ROS generation.[10] Ran prepared a hyaluronidase-triggered bactericidal photothermal platform based on silver nanodroplets and graphene oxide with excellent antibacterial properties against *S. aureus*.[11] Zhao embedded hydrophilic ZnO nanoparticles into calcium alginate hydrogels to form composite material that was 99% bactericidal against *E. coli* and *S. aureus* in water under ambient light.[12] However, these metallic droplets not widely used as antimicrobial agents because of their high cost, contamination, and cytotoxicity.[13]

As part of an organism's innate immune system, antimicrobial peptides are considered to be excellent alternatives to traditional antibiotics. Park prepared a new antimicrobial agent assembled from a chimeric antimicrobial peptide and an amphiphilic degradable polymer that can effectively target and disrupt bacterial membranes and kill many bacteria.[14] The lack of

[a]*Institute of Translational Medicine, Medical College, Yangzhou University, Yangzhou, 225009, China. E-mail: liuqi@yzu.edu.cn; chenjing2018@yzu.edu.cn; Tel: +86-514-87992233*

[b]*Jiangsu Key Laboratory of Integrated Traditional Chinese and Western Medicine for Prevention and Treatment of Senile Diseases, Yangzhou University, Yangzhou, 225009, China*

[c]*College of Horticulture and Plant Protection, Yangzhou University, Yangzhou, 225009, China. E-mail: jgfeng@yzu.edu.cn; Tel: +86-514-87979395*

widespread use of designed antimicrobial peptides is attributed to high commodity costs, resistance to proto-proteolytic degradation, and unknown toxicological profiles when systematically administered.[15] Phototherapy has also matured,[16] with Mao using a black phosphorus-based hydrogel for photodynamic therapy to enhance skin cell proliferation and differentiation and promote the healing of bacterially infected wounds.[17] With the growing global concern about microbial infections, the development of new inexpensive and biocompatible antimicrobial agents as alternatives has become essential.

Essential oils are secondary metabolites of plants with a strong aromatic odor, volatile at room temperature, and found mainly in the roots, shoots, stems and leaves of plants.[18] In many essential oils, eugenol (4-allyl-2-methoxyphenol) is an essential oil that can be obtained from various plants and is one of the main components of clove oil, which has pharmacological activities, such as anaesthetic,[19] anti-inflammatory,[20] antioxidant[20] and anti-cancer[21] in which the antibacterial activity is prominent.[22] Hayriye has designed and synthesized eugenol oxypropanolamine derivatives that have inhibitory effects on a wide range of drug-resistant bacteria and are antidiabetic and anticholinergic.[23] However, the high volatility and low water solubility of eugenol greatly limit its clinical application. Therefore, how to improve the stability of eugenol and effectively utilize the antibacterial function of eugenol is currently the focus in the medical field. Loading eugenol into nanopolymeric materials remarkably improves its stability and antibacterial activity.[24,25] However, these methods are not only cumbersome, but also increase the cost of preparation.

Nanoemulsions are non-thermodynamically stable colloidal dispersions that can be divided into three types, namely, W/O, O/W, and bicontinuous, depending on whether oil or water is used as the dispersed phase.[26] Nanoemulsions have good kinetic stability, and the presence of emulsifiers and other co-emulsifiers in the emulsion reduces oil–water interfacial tension.[27] The droplet diameter ranges from 30 nm to 200 nm, and the nanoscale droplet diameter reduces droplet aggregation, flocculation, and gravitational effects, thus significantly improving emulsion stability.[28] Eugenol emulsions emulsified with cinnamaldehyde/chitosan and glycerol monocapsules as co-stabilizers have long-term stability and excellent antibacterial activity.[29] Therefore, the antibacterial activity of eugenol can be improved by preparing it as a highly dispersed and permeable nanoemulsion.

In this study, eugenol nanoemulsions with good stability were developed using an efficient delivery system, eugenol as the oil phase, and Tween-80 as the single surfactant. Our investigation compared the inhibitory effect and mechanism of the optimized nanoemulsion against *E. coli* and *S. aureus*. It was also evaluated for safety by cytotoxicity testing and flow cytometry.

Materials and methods

Materials

Eugenol with a purity (≥99%) was obtained from Jiangxi Cedar Natural Medicinal Oil Co., Ltd (Anji, China). Tween-20 (T20), Tween-40 (T40), Tween-60 (T60), and Tween-80 (T80) were obtained from Jiangsu Haian Petroleum Chemical Factory (Haian, China). *E. coli* and *S. aureus* were provided by Medical College of Yangzhou University. The reactive oxygen species (ROS), malondialdehyde (MDA), and Cell Counting Kit-8 (CCK-8) test kits were obtained from Beyotime Biotechnology (Shanghai, China). BEAS-2B and L02 were provided by Shanghai Biowing Applied Biotechnology Co. Ltd. (Shanghai, China). Annexin V-FITC/PI apoptosis detection kit was provided by Procell Life Science and Technology Co., Ltd. (Wuhan, China).

Preparation of nanoemulsions

High shear mixer (IKA, Germany) was used for the preparation of nanoemulsions as previously described.[30] First, coarse emulsion was prepared with mixing 5% (w/w) essential oil and surfactant by using a magnetic stirrer for 10 min at 1000 rpm at room temperature. Then, deionized water was added to the oil phase, the final volume was adjusted to 100% (w/w), and the mixture was treated by a high shear mixer at 12 000 rpm. The prepared nanoemulsion was then transferred to three reagent bottles. The effect of types, concentrations of surfactants, and shearing times on the stability of the nanoemulsions was evaluated.

Visual inspection

Nanoemulsions were stored at 0 ± 2 °C for 7 days and at 54 ± 2 °C for 14 days, then the change in visual inspection was observed in comparison with the freshly prepared samples. Phenomena such as phase emulsification, separation, precipitation and flocculation imply instability of the nanoemulsions.

Characterization of nanoemulsions

Dynamic light scattering. Measurements were carried out by using a dynamic light scattering droplet diameter analyzer (ZS90 Nano, Malvern Instruments Co., Ltd., England). The nanoemulsion was diluted 200-fold with distilled water before measuring. The measurement was repeated thrice for each sample, and the average value was obtained.

Confocal laser scanning microscopy. The microstructures of the nanoemulsions were observed using a confocal laser scanning microscopy. Exactly 20 μL of 1 mg μL^{-1} fluorescein was added to 20 mL of sample and mixed thoroughly, then 10 μL of stained nanoemulsion was added dropwise to the slide. The samples were observed using a confocal laser scanning microscopy with a 40× objective.

Antibacterial activities and mechanism

Microbiological test. The inhibitory effect was evaluated by plate counting method. The culture method of colony was in accordance with Louise.[25] Then, 1 mL of bacterial suspension of each bacterial strain was added in each tube, including eugenol nanoemulsion. The final concentrations of the sample were 0.02, 0.04, 0.06, 0.08, and 0.1 mg μL^{-1}. The control group only added 0.02 mg μL^{-1} nanoemulsions without eugenol. Serial dilution in deionized water was done for each sample. Each diluted sample (100 μL) was surface-plated on individual glucose agar plates. Two plates were used for each sample. The

plates were cultured at 37 °C for 1 day, then the colonies were counted.

Scanning electron microscopy. Bacterial samples were treated with glutaraldehyde at 0 °C for 12 h and then centrifuged to remove the supernatant. Then dehydrate the samples with graded concentrations of ethanol (30%, 50%, 70%, 80%, 90%, 95%, and 100% v/v). The dried samples are subjected to critical point drying and gold spraying operations. Scanning electron microscopy (SEM) was carried out to observe changes in bacterial morphology.

Measurement of protein leakage. Protein leakage was performed as described by Mao.[31] Initially, *E. coli* and *S. aureus* were washed and suspended with PBS. The bacterial suspensions were cultured with 0.1 and 0.5 mg μL^{-1} nanoemulsion for 2 h. The control group only added 0.1 mg μL^{-1} nanoemulsions without eugenol. The bacterial suspensions cultured with PBS were used as controls. The protein leakage of each sample was determined by microplate reader at OD562.

ROS and MDA detection of the bacteria. The bacteria were cultured as described above, the bacterial suspension (1 mL) was collected and added with DCFH-DA (2′,7′-dichlorofluorescin diacetate) fluorescent probe (1 μL). After incubation for 30 min, the supernatant was removed by centrifugation for three times. Approximately 1 mL of 0.2 mg μL^{-1} of nanoemulsion was added to the experimental group, and 1 mL of 0.2 mg μL^{-1} nanoemulsion without eugenol was added to the control group. The excitation wavelength of ROS test was 488 nm and the emission wavelength was 525 nm.

Approximately 200 μL of nanoemulsions at concentrations of 0.1, 0.2, 0.3, 0.4, and 0.5 mg μL^{-1} were mixed with the prepared assay reagents and heated at 95 °C for 40 min. Then, the sample was centrifuged at 3500 rpm for 12 min. At last, the supernatant was obtained, and the absorbance was measured at 532 nm. The percentage of MDA was calculated according to the following formula (1):

$$\text{Percentage of MDA} = \frac{(OD_M - OD_B)}{(OD_S - OD_B)} \times 100\% \quad (1)$$

OD_M is the measured value; OD_S is the standard value; OD_B is the blank value.

Safety evaluation

Cytotoxicity assay. Biocompatibility was another concern in this study. BEAS-2B and L02 were selected as subjects to investigate the effects of eugenol nanoemulsions on the respiratory and digestive tracts. The cytotoxicity of BEAS-2B and L02 was assessed by CCK-8 assay. The cell culture method was performed as described by Fan.[32] The BEAS-2B and L02 cells were distributed into 96-well plates with a density of 5×10^4 cells per well, and nanoemulsion was applied at 0.025, 0.05, 0.1, 0.2, and 0.4 mg L^{-1} for 24 and 48 h. After incubation, standard CCK-8 treatment was performed to determine the relative cell viabilities. The optical density (OD) values were measured at 450 nm. Survival rate was calculated according to the following formula (2):

$$\text{Survival rate} = \frac{\text{sample value} - \text{negative control}}{\text{positive control} - \text{negative control}} \times 100\% \quad (2)$$

Flow cytometry analysis. The types of cell death induced by eugenol nanoemulsion in BEAS-2B and L02 cells were determined by FACS (BD FFACS Calibur, USA) analysis. BEAS-2B cells and L02 were seeded into six-well plates, with a density of 1×10^6 cells per well. After treatment with eugenol nanoemulsion at 0.025, 0.05, and 0.1 mg L^{-1}, cells were resuspended in 100 μL of binding buffer, 5 μL of Annexin V-FITC, and 10 μL of PI and incubated for 15 min at room temperature. Approximately 400 μL binding buffer was added, and the staining was detected using flow cytometry.

Statistical analysis. There were at least 3 replicates for all measurements and data were presented as mean ± SD. The differences were considered significant when the p values were below 0.05. All statistical analyses were performed using the SPSS Version 22.0 for Windows (IBM SPSS Inc., Chicago, IL).

Results and discussion

Evaluation of stability

Effect of surfactant type. The choice of a suitable surfactant is an important factor for the formulation of nanoemulsions.[33] The hydrophile–lipophile balance (HLB) indicates the hydrophilic and hydrophobic properties of a surfactant. Stable oil-in-water nanoemulsions can be manufactured using a surfactant with a high HLB value.[34,35] The most stable nanoemulsion is obtained when the HLB values of the surfactant and the emulsified oil phase are close.[36] Four surfactants, namely, T20, T40, T60 and T80, were used in this study with HLB values of 16.5, 15.5, 14.5, and 15, respectively.

Fig. 1a shows the visual inspection of nanoemulsions prepared by different surfactants at different storage temperatures. After fresh preparation, the T40 nanoemulsion was pale blue and translucent, and the other samples were pale white and opaque. After storage at low temperature, the oil droplets of the T20 nanoemulsion settled to the bottom of the bottle, the T80 nanoemulsion was pale blue and translucent, and the other samples were milky white and opaque. After storage at high temperature, both the T20 and T60 nanoemulsions exhibited phase separation. The T40 nanoemulsion exhibited slight coalescence at the bottom. By contrast, the T80 nanoemulsion is milky white and opaque with no instability such as coalescence or sediment, indicating its good stability.

Fig. 1b shows microscopic photographs of the nanoemulsions prepared by different surfactants after fresh preparation. Only the T80 nanoemulsion showed small and homogeneous droplets, while the T20 and T60 nanoemulsions had large and unevenly distributed droplets. The T40 nanoemulsion exhibited a tendency for localized droplet aggregation, confirming the coalescence phenomenon described above.

Fig. 1c shows the average droplet diameter of nanoemulsions prepared using different surfactants at different storage temperatures. After fresh preparation, the T80

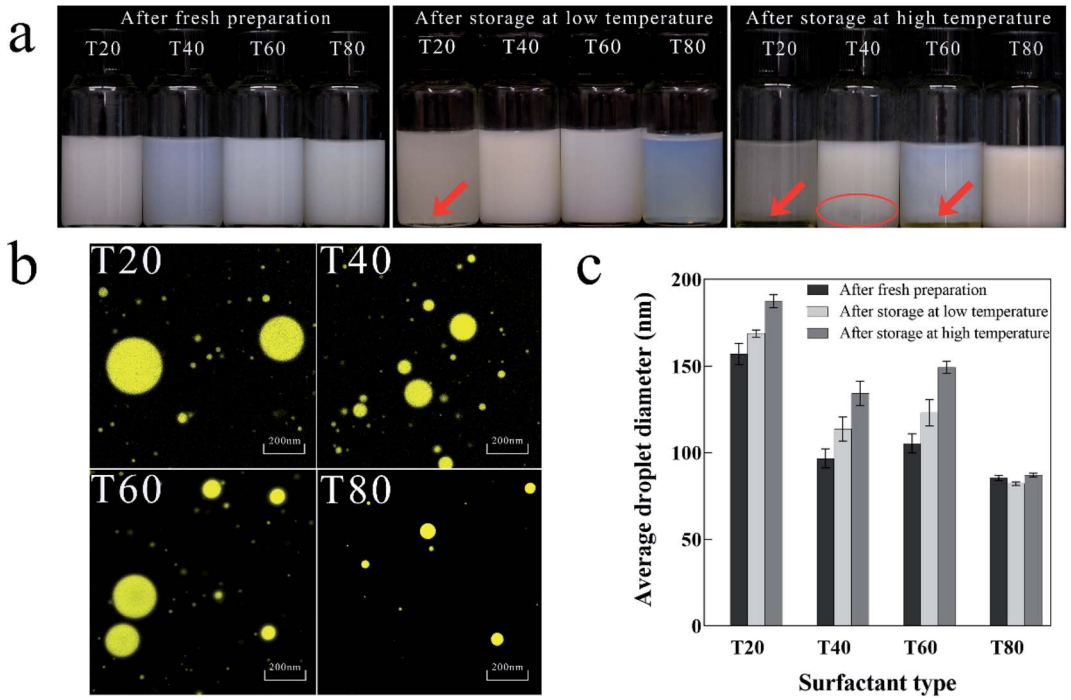

Fig. 1 Physical properties of nanoemulsion prepared by different surfactants. (a) Visual inspection after fresh preparation, storage at low and high temperature; (b) microscopic photograph after fresh preparation; (c) variations in average droplet diameter after fresh preparation, storage at low and high temperature.

nanoemulsion had the smallest average droplet diameter (85 nm), while the T20 nanoemulsion had the highest (155 nm). After storage at low and high temperatures, the average droplet diameter of the T80 nanoemulsion did not vary significantly, whereas the average droplet diameter of the nanoemulsions prepared by the remaining surfactants increased significantly.

The experimental results show that T80 is more suitable for the preparation of stable nanoemulsion, probably because the HLB value of T80 is closer to that of eugenol. Niyaz Ahmad[37] also found in their study of eugenol nanoemulsion that the use of T80 as a surfactant was effective in reducing the droplet diameter and stabilizing the nanoemulsion.

Effect of surfactant concentration. The appropriate surfactant concentration is essential for the formation of stable nanoemulsion.[38] Fig. 2a shows the visual inspection of nanoemulsions prepared by different surfactant concentrations at different storage temperatures. The 10% T80 nanoemulsion was pale blue and translucent, while the others were pale white and opaque. After storage at low temperature, the 8% T80 nanoemulsion was bluer and more transparent than the 10% T80 nanoemulsion, and the other nanoemulsions were milky white and opaque. After storage at high temperature, the 4% T80 nanoemulsion showed a distinct oil layer at the bottom and turned greyish white, while the 6% T80 nanoemulsion slightly coalesced at the bottom. The 8% and 10% T80 nanoemulsions both remained stable, but the 10% T80 nanoemulsion adhered more easily to the glass bottle wall than 8% T80 nanoemulsion. The results showed that the 8% T80 nanoemulsion had low viscosity and good stability.

Fig. 2b shows the microscopic photographs of the nanoemulsions prepared using different surfactant concentrations after fresh preparation. The droplets of 4% and 6% T80 nanoemulsions were large and uneven. The droplets of 8% and 10% T80 nanoemulsions were small and evenly distributed.

Fig. 2c shows the average droplet diameters of nanoemulsions prepared with different surfactant concentrations at different storage temperatures. After fresh preparation, the average droplet diameter of the nanoemulsion decreased as the concentration of the surfactant increased. The 10% T80 nanoemulsion had the lowest average particle diameter (70 nm), followed by the 8% T80 nanoemulsion (85 nm). After storage at low and high temperatures, the 8% T80 nanoemulsion showed the smallest variation in droplet diameter (±5 nm). The other nanoemulsions showed droplet diameter variations in the range of ±50 nm, illustrating their instability over prolonged storage.

Hence, with the increase in surfactant concentration, the droplets of the nanoemulsion become smaller, more uniformly distributed, and show better stability.[39] Surfactants favor the preparation of nanoemulsion with smaller droplets to increase the amount of adsorption around the oil–water interface of the droplet and to reduce the internal tension of the system.[40,41] Thereby, when the concentration of surfactant ranges from 4% to 6%, larger droplets are obtained, because the concentration is very low to achieve the necessary stability of the system. When surfactant concentration ranges from 8% to 10%, the droplet diameters of the nanoemulsion do not vary greatly and are stable after fresh preparation. However, after prolonged storage,

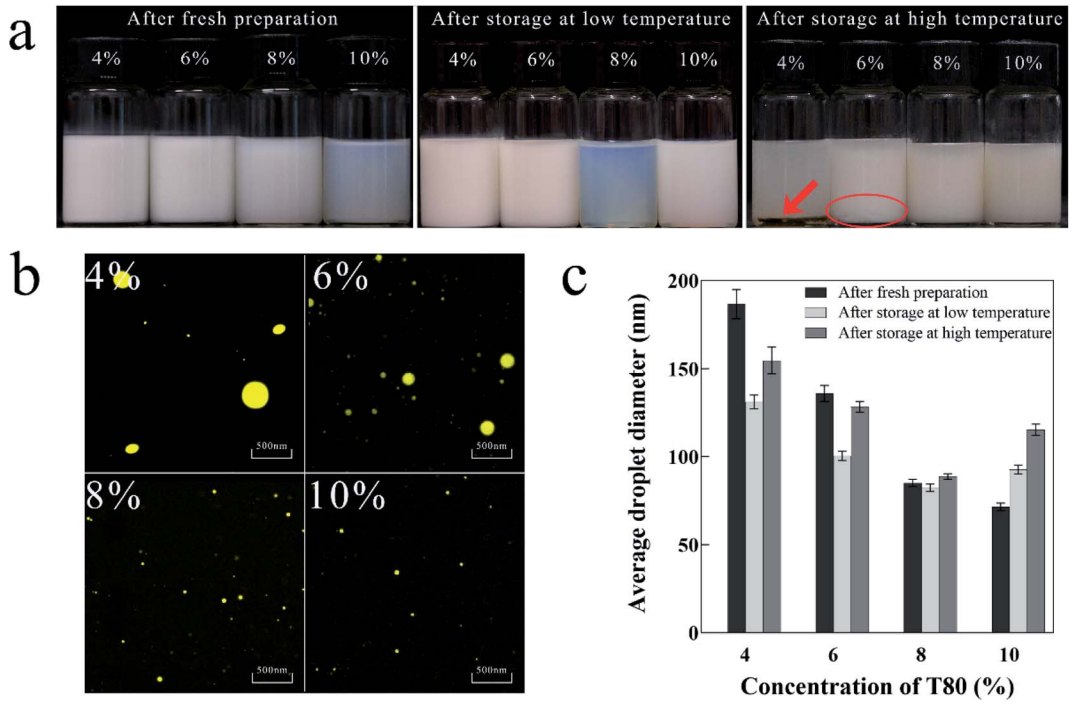

Fig. 2 Physical properties of nanoemulsion prepared with different surfactant concentrations. (a) Visual inspection after fresh preparation and storage at low and high temperature; (b) microscopic photograph after fresh preparation; (c) variations in average droplet diameter after fresh preparation and storage at low and high temperature.

the droplet diameter of 10% T80 nanoemulsion increased, and this instability may be attributed to Ostwald ripening.[42] The difference in solubility between large and small droplets results in the formation of larger droplets at the cost of small droplets. This phenomenon has been previously reported.[43,44]

Effect of shearing time. Fig. 3a shows the visual inspection of the nanoemulsions with different shearing times at different storage temperatures. After fresh preparation, nanoemulsions with different shearing times were all stable and had milky white color. After storage at low temperature, the nanoemulsion with shearing time of 5 min was pale blue and transparent, while the nanoemulsion with shearing times of 3 and 7 min were milky and opaque. After storage at high temperature, it is noteworthy that the nanoemulsion with shearing times of 3 and 7 min showed significant flocculation in the upper part of reagent bottles, and only the nanoemulsion with shearing time of 5 min remained stable.

Fig. 3b shows the microscopic photographs of the nanoemulsions with different shearing times after fresh preparation. In addition to the locally larger droplets and uneven distribution in the nanoemulsion with shearing time of 3 min, the droplets of the nanoemulsions with other shearing times are all small and uniformly distributed.

Fig. 3c shows the average droplet diameters of nanoemulsions with different shearing times at different storage temperatures. After fresh preparation, the nanoemulsion with shearing time of 5 min had the smallest droplet diameter (85 nm), whereas that with shearing time of 3 min had the largest droplet diameter (145 nm). After storage at low and high temperatures, the nanoemulsion with shearing time of 5 min had the smallest variation in droplet diameter (±5 nm), while the two remaining groups had a large variation in droplet diameter. The nanoemulsions with shearing time of 7 min may have aggregated and had increased diameter despite the smaller droplets after fresh preparation.

Hence, the nanoemulsion with shearing time of 5 min was relatively stable. The length of the shearing time affects the energy provided by shearing.[45] The short shearing time (3 min) provides insufficient shearing energy, resulting in large droplet diameters and non-uniform distribution of the nanoemulsion. The long shearing time (7 min) increases the probability of collision of nanoemulsion droplets, thus increasing the frequency of coalescence at high energy, causing an increase in the average droplet diameter.[46]

Determination of the formulation

Based on above results, the nanoemulsion prepared by 8% T80 and 5 min shearing time was the optimal formulation with good physical properties. To investigate its antibacterial activities and safety, we performed the following experiments.

Antibacterial activities and mechanism

Microbiological test against *E. coli* and *S. aureus*. The antibacterial activities of eugenol nanoemulsion were investigated in this study. Therefore, the study tested the broad-spectrum antibacterial properties of eugenol nanoemulsion through Gram-negative (*E. coli*) and Gram-positive (*S. aureus*) bacterial

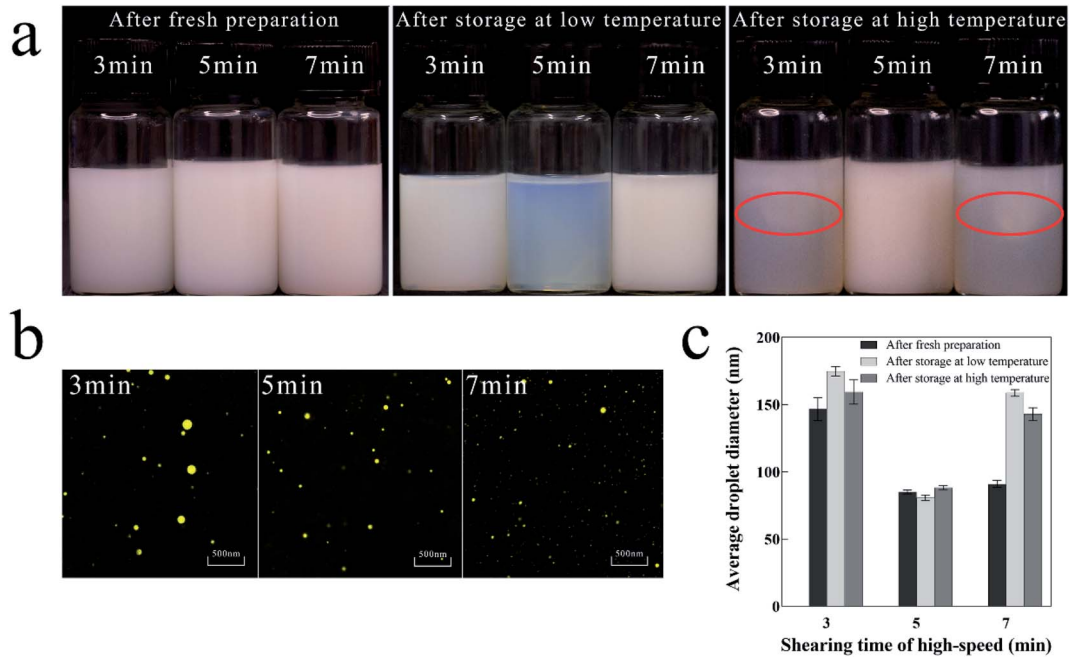

Fig. 3 Physical properties of nanoemulsion with different shearing times. (a) Visual inspection after fresh preparation, storage at low and high temperature; (b) microscopic photograph after fresh preparation; (c) variations in average droplet diameter after fresh preparation and storage at low and high temperature.

inhibition assays (Fig. 4). The experimental groups treated by different concentrations of eugenol nanoemulsion showed an exponential decrease in colony counts compared with the blank control group (nanoemulsions without eugenol). The same concentration of eugenol nanoemulsion prepared by T80 inhibited *E. coli* much more than *S. aureus* and the same result was found by Li.[47] Meanwhile, they found the antibacterial activity of eugenol nanoemulsion was affected by the surfactant type, non-ionic surfactant T80 was more sensitive to *E. coli*. Furthermore, some researchers indicated surfactants play a role in the process of nanoemulsion antibacterial activity by affecting on bacterial cell membranes. Ryu[48] found T80 can increase the effective delivery of essential oil to the cell membrane due to its low negative charge on the surface and weak electrical repulsion on the bacterial membrane surface.

Antibacterial mechanism. In addition, bacterial morphological images were obtained by SEM to effectively describe the possible disruption of bacteria treated by the nanoemulsions. Fig. 5a shows that the control *E. coli* showed a regular rod shape, while the bacteria treated with nanoemulsion underwent significant deformation accompanied by membrane rupture and leakage of contents. Fig. 5b shows that the control *S. aureus*

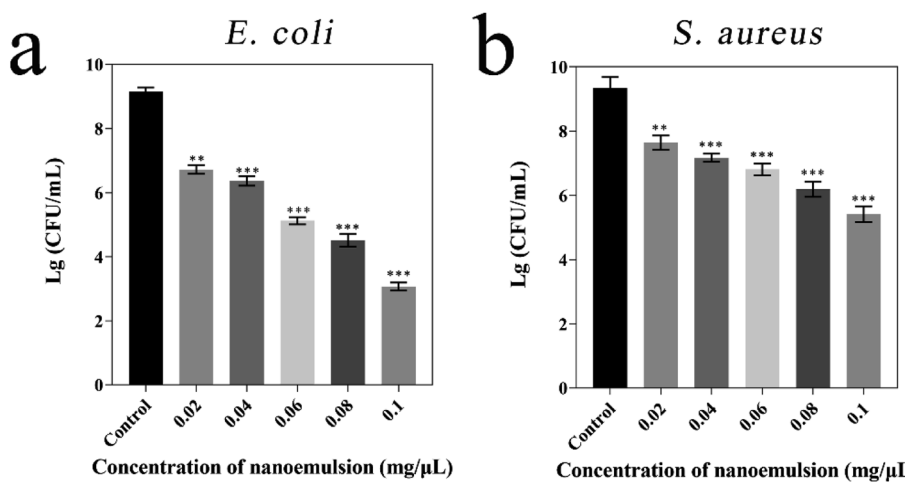

Fig. 4 Microbiological test of nanoemulsion against *E. coli* (a) and *S. aureus* (b). Compared with the control group, *p* values in all experimental groups were below 0.05.

had a smooth and complete surface, while after treatment, the bacteria adhered to each other, most bacteria were severely deformed, and some of them ruptured and their contents leaked. Hence, the antibacterial activity of the nanoemulsions is achieved primarily through the penetration and disruption of bacterial membranes.

To further validate this conclusion, we performed optical density measurements at 562 nm as shown in Fig. 5c and d, indicating leakage of bacterial proteins. The optical density values of *E. coli* and *S. aureus* suspensions treated by 0.1 mg μL^{-1} nanoemulsion were 0.43 and 0.171, respectively. When the concentration is 0.5 mg μL^{-1}, the optical density values were 0.79 and 0.37. Thus, the protein leakage of *E. coli* was evident, confirming our previous inhibition experiments. Bejrapha[49] performed membrane permeability experiments on *E. coli*, and also found that the amount of content leakage depends on the increase in concentration of eugenol nanoemulsions which may reduce hydrophobicity of bacterial surfaces, thus damaging cell membranes and causing content leakage.

Reactive oxygen species (ROS) are caused by blocked electron transport along the respiratory chain in damaged plasma membranes, which enhanced lipid peroxidation and cause tissue damage. Malondialdehyde (MDA) is the metabolised of lipid peroxidation that reflects the degree of lipid peroxidation. To further explore the mechanism of bacterial inhibition, the ROS and MDA levels before and after bacterial treatment were tested. Fig. 6a and c showed that ROS levels in *E. coli* treated by 0.1 mg μL^{-1} nanoemulsion were 4×10^5 a.u. higher, and ROS levels in *S. aureus* were about 5×10^4 a.u. over higher to comparing the control group. Fig. 6b and d showed that MDA induced by ROS reached 648% in *E. coli* and 583% in *S. aureus* when treated by 0.5 mg μL^{-1} nanoemulsion. Balaram[50] and Sun[51] *et al.* also found there were significant increase in ROS levels in *S. aureus* and *E. coli* when they treated these two bacteria with eugenol. More research shows ROS attack the membrane integrity and morphology of both bacteria, significantly increasing membrane permeability and ultimately causing intracellular leakage.[52,53]

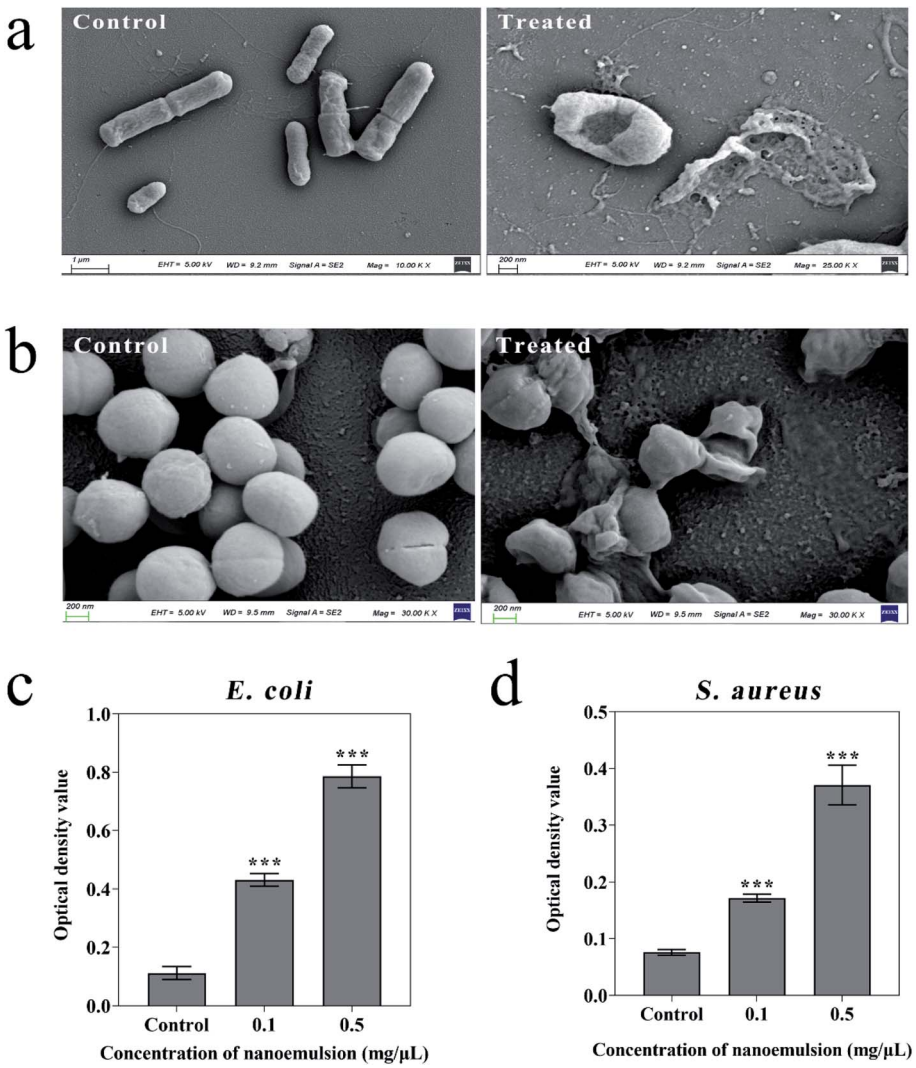

Fig. 5 Microscopic morphology of *E. coli* (a) and *S. aureus* (b) before and after nanoemulsion treatment; the protein leakage from *E. coli* (c) and *S. aureus* (d) induced by nanoemulsion. Compared with the control group, *p* values in all experimental groups were below 0.05.

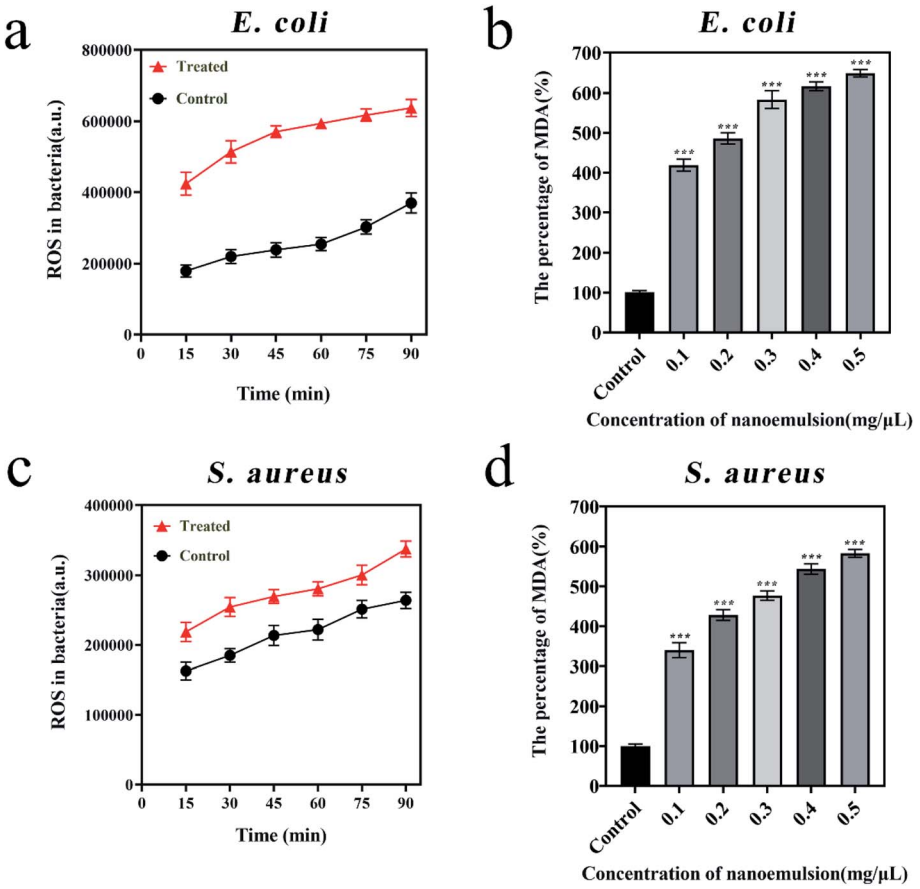

Fig. 6 Variations in ROS levels in *E. coli* (a) and *S. aureus* (c); variations in MDA levels in *E. coli* (b) and *S. aureus* (d). Compared with the control group, *p* values in all experimental groups were below 0.05.

Safety evaluation

Cytotoxicity assay on BEAS-2B and L02. To evaluate whether the optimized nanoemulsion has cytotoxic effects, we treated BEAS-2B and L02 with a certain concentration of nanoemulsion (0.025–0.4 mg L^{-1}). The survival rates of BEAS-2B and L02 were greater than 90% after 24 h of treatment at 0.025 mg L^{-1}. The survival rates of L02 were less than that of BEAS-2B at the same concentration, indicating that the nanoemulsion was more

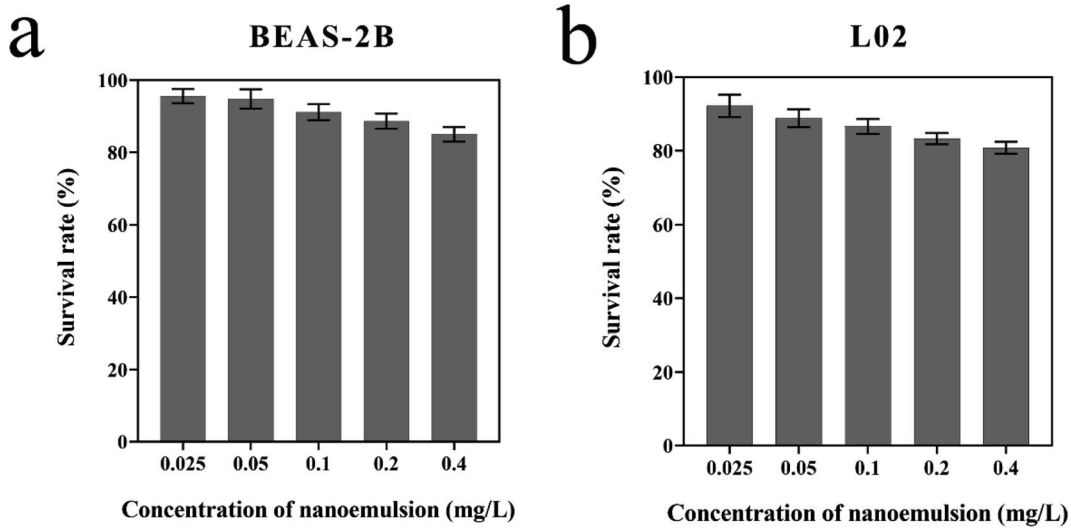

Fig. 7 Survival rate of BEAS-2B (a) and L02 (b) treated by nanoemulsion.

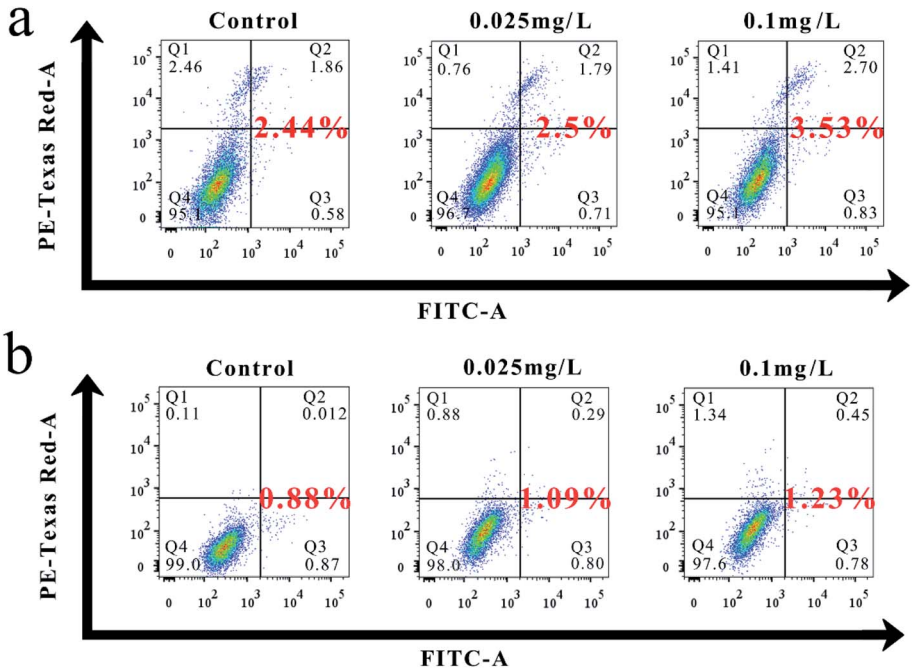

Fig. 8 (a) Effect of nanoemulsion on the apoptosis of BEAS-2B. (b) Effect of nanoemulsion on the apoptosis of L02.

toxic to L02 than to BEAS-2B. Nanoemulsion slightly reduced the survival rates of BEAS-2B and L02 at 0.025–0.4 mg L^{-1}, in which all survival rates were greater than 80%. The results show that the optimized nanoemulsion has good biocompatibility and has low toxicity to BEAS-2B and L02 (Fig. 7).

Flow cytometry analysis. Fig. 8a and b show the flow cytometric analysis results, indicating that the total apoptotic rates of BEAS-2B and L02 treated with different concentrations of nanoemulsion for 24 h increased slightly compared with the untreated control. The total apoptosis rates of BEAS-2B treated by 0.025 and 0.1 mg L^{-1} nanoemulsions were 2.5% and 3.53%, which were 1.02 and 1.45 times higher than that of the control, respectively. By comparison, the total apoptosis rate of L02 was 1.24 and 1.4 times higher than that of the control. Hence, the effect of nanoemulsion on the total apoptosis of BEAS-2B was more pronounced than that of L02.

Conclusion

In this study, we demonstrated a reliable method for the preparation of stabilized eugenol nanoemulsion, explored its antibacterial effect and mechanism against *E. coli* and *S. aureus*, and examined its biocompatibility. The nanoemulsion prepared by mixing 5% (w/w) eugenol and 8% (w/w) T80 after 5 min of shearing was stable at different storage temperatures with small and homogeneous droplet diameter. The results of the bacterial inhibition tests showed that the nanoemulsion was highly inhibitory to both bacteria, in which Gram-negative bacteria was more effectively inhibited than positive bacteria. SEM and protein leakage assay experiments initially showed that the nanoemulsion ruptured the cell membrane and leaked the contents. The increased levels of ROS and MDA further revealed that lipid peroxidation occurred in the bacteria because of nanoemulsion, and this phenomenon altered the permeability and disrupted the structure of the cell membrane. Cytotoxicity tests and flow cytometry results showed no significant effect of the nanoemulsion on the proliferation and apoptosis of L02 and BEAS-2B, indicating the low toxicity and good biocompatibility of the nanoemulsion. The results of this study can provide an efficient, low toxicity, and safe delivery system for the promotion and application of relevant plant essential oils with antibacterial activity such as wound therapy.

Author contributions

Xuan Fu: conceptualization, supervision, project administration, data curation, investigation. Yuan Gao: formal analysis, software, methodology, data curation. Weiyao Yan: conceptualization, supervision, project administration, data curation, investigation. Ziluo Zhang: formal analysis, software, methodology, data curation. Shovra Sarker: formal analysis, software, methodology, data curation. Yinyan Yin: formal analysis, software, methodology, data curation. Qi Liu: conceptualization, investigation, formal analysis, data curation, writing – original draft, writing – review & editing, funding acquisition. Jianguo Feng: conceptualization, investigation, formal analysis, data curation, writing – original draft, writing – review & editing, funding acquisition. Jing Chen: conceptualization, investigation, formal analysis, data curation, writing – original draft, writing – review & editing, funding acquisition.

Conflicts of interest

The authors declare that they have no known competing financial interests or personal relationships that could have appeared to influence the work reported in this paper.

Acknowledgements

This research was funded by the Innovation and Entrepreneurship Training Program for College Students (X20210756) by Yangzhou University; the Traditional Chinese Medicine Science and Technology Development Project of Jiangsu Province (Grant No. YB201994); the Agricultural Science and Technology Innovation Fund in Jiangsu Province (CX(19)3112). Thanks for the professional test provided by Yangzhou University Test Center.

References

1 A. S. Fauci and D. M. Morens, *N. Engl. J. Med.*, 2012, **366**, 454–461.
2 D. M. Morens, G. K. Folkers and A. S. Fauci, *Lancet Infect. Dis.*, 2008, **8**, 710–719.
3 A. Darfeuille-Michaud, J. Boudeau, P. Bulois, C. Neut, A.-L. Glasser, N. Barnich, M.-A. Bringer, A. Swidsinski, L. Beaugerie and J.-F. Colombel, *Gastroenterology*, 2004, **127**, 412–421.
4 C. Liu, A. Bayer, S. E. Cosgrove, R. S. Daum, S. K. Fridkin, R. J. Gorwitz, S. L. Kaplan, A. W. Karchmer, D. P. Levine, B. E. Murray, M. J. Rybak, D. A. Talan and H. F. Chambers, *Clin. Infect. Dis.*, 2011, **52**, E18–E55.
5 K. L. Greathouse, J. K. Stone and C. C. Harris, *Cancer Cell*, 2020, **38**, 158–160.
6 R. H. Hunt, M. Camilleri, S. E. Crowe, E. M. El-Omar, J. G. Fox, E. J. Kuipers, P. Malfertheiner, K. E. L. McColl, D. M. Pritchard, M. Rugge, A. Sonnenberg, K. Sugano and J. Tack, *Gut*, 2015, **64**, 1650.
7 J. Davies and D. Davies, *Microbiol. Mol. Biol. Rev.*, 2010, **74**, 417–433.
8 P. S. Stewart and J. W. Costerton, *Lancet*, 2001, **358**, 135–138.
9 S. B. Levy and B. Marshall, *Nat. Med.*, 2004, **10**, S122–S129.
10 Y. Li, W. Zhang, J. Niu and Y. Chen, *ACS Nano*, 2012, **6**, 5164–5173.
11 X. Ran, Y. Du, Z. Z. Wang, H. Wang, F. Pu, J. S. Ren and X. G. Qu, *ACS Appl. Mater. Interfaces*, 2017, **9**, 19717–19724.
12 W.-B. Zhao, M.-R. Du, K.-K. Liu, R. Zhou, R.-N. Ma, Z. Jiao, Q. Zhao and C.-X. Shan, *ACS Appl. Mater. Interfaces*, 2020, **12**, 13305–13315.
13 F. Alessandrini, A. Vennemann, S. Gschwendtner, A. U. Neumann, M. Rothballer, T. Seher, M. Wimmer, S. Kublik, C. Traidl-Hoffmann, M. Schloter, M. Wiemann and C. B. Schmidt-Weber, *Nanomaterials*, 2017, **7**, 300.
14 S.-C. Park, C. Ko, H. Hyeon, M.-K. Jang and D. Lee, *ACS Appl. Mater. Interfaces*, 2020, **12**, 54306–54315.
15 R. E. W. Hancock and H. G. Sahl, *Nat. Biotechnol.*, 2006, **24**, 1551–1557.
16 Y. Q. Wang, Y. Y. Jin, W. Chen, J. J. Wang, H. Chen, L. Sun, X. Li, J. Ji, Q. Yu, L. Y. Shen and B. L. Wang, *Chem. Eng. J.*, 2019, **358**, 74–90.
17 C. Y. Mao, Y. M. Xiang, X. M. Liu, Z. D. Cui, X. J. Yang, Z. Y. Li, S. L. Zhu, Y. F. Zheng, K. W. K. Yeung and S. L. Wu, *ACS Nano*, 2018, **12**, 1747–1759.
18 F. Bakkali, S. Averbeck, D. Averbeck and M. Waomar, *Food Chem. Toxicol.*, 2008, **46**, 446–475.
19 C. K. Park, K. Kim, S. J. Jung, M. J. Kim, D. K. Ahn, S. D. Hong, J. S. Kim and S. B. Oh, *Pain*, 2009, **144**, 84–94.
20 B. Yogalakshmi, P. Viswanathan and C. V. Anuradha, *Toxicology*, 2010, **268**, 204–212.
21 I. Al-Sharif, A. Remmal and A. Aboussekhra, *BMC Cancer*, 2013, **13**, 600.
22 A. Marchese, R. Barbieri, E. Coppo, I. E. Orhan, M. Daglia, S. F. Nabavi, M. Izadi, M. Abdollahi, S. M. Nabavi and M. Ajami, *Crit. Rev. Microbiol.*, 2017, **43**, 668–689.
23 H. G. Bilgicli, A. Kestane, P. Taslimi, O. Karabay, A. Bytyqi-Damoni, M. Zengin and I. Gulcin, *Bioorg. Chem.*, 2019, **88**, 7.
24 A. Celebioglu and T. Uyar, *Food Hydrocolloids*, 2021, **111**, 106264.
25 L. Breloy, C. A. Ouarabi, A. Brosseau, P. Dubot, V. Brezova, S. Abbad Andaloussi, J.-P. Malval and D.-L. Versace, *ACS Sustain. Chem. Eng.*, 2019, **7**, 19591–19604.
26 Y. Singh, J. G. Meher, K. Raval, F. A. Khan, M. Chaurasia, N. K. Jain and M. K. Chourasia, *J. Controlled Release*, 2017, **252**, 28–49.
27 N. Salim, N. Ahmad, S. H. Musa, R. Hashim, T. F. Tadros and M. Basri, *RSC Adv.*, 2016, **6**, 6234–6250.
28 L. Salvia-Trujillo, R. Soliva-Fortuny, M. A. Rojas-Graü, D. J. McClements and O. Martín-Belloso, *Annu. Rev. Food Sci. Technol.*, 2017, **8**, 439–466.
29 R. N. Zhao, R. Song, G. G. Sun, S. L. Liu, B. Li, Y. P. Cao and Y. Li, *Food Hydrocolloids*, 2020, **107**, 10.
30 Q. Liu, Y. Gao, X. Fu, W. Chen, J. Yang, Z. Chen, Z. Wang, X. Zhuansun, J. Feng and Y. Chen, *Colloids Surf., B*, 2021, **201**, 111626.
31 C. Mao, Y. Xiang, X. Liu, Y. Zheng, K. W. K. Yeung, Z. Cui, X. Yang, Z. Li, Y. Liang, S. Zhu and S. Wu, *ACS Appl. Mater. Interfaces*, 2019, **11**, 17902–17914.
32 X. Fan, F. Yang, C. X. Nie, Y. Yang, H. F. Ji, C. He, C. Cheng and C. S. Zhao, *ACS Appl. Mater. Interfaces*, 2018, **10**, 296–307.
33 D. O. Grigoriev and R. Miller, *Curr. Opin. Colloid Interface Sci.*, 2009, **14**, 48–59.
34 I. K. Hong, S. I. Kim and S. B. Lee, *J. Ind. Eng. Chem.*, 2018, **67**, 123–131.
35 Y. Chen, H. Y. Zhang, J. Yang and H. Y. Sun, *Molecules*, 2015, **20**, 21167–21177.
36 Y. Liu, F. Wei, Y. Wang and G. Zhu, *Colloids Surf., A*, 2011, **389**, 90–96.
37 N. Ahmad, F. J. Ahmad, S. Bedi, S. Sharma, S. Umar and M. A. Ansari, *Saudi Pharm. J.*, 2019, **27**, 778–790.
38 P. Chuesiang, U. Siripatrawan, R. Sanguandeekul, L. McLandsborough and D. Julian McClements, *J. Colloid Interface Sci.*, 2018, **514**, 208–216.
39 L. Y. Zeng, X. Xin and Y. L. Zhang, *RSC Adv.*, 2017, **7**, 19815–19827.
40 L.-C. Peng, C.-H. Liu, C.-C. Kwan and K.-F. Huang, *Colloids Surf., A*, 2010, **370**, 136–142.
41 K. Nakabayashi, H. Yanagi and M. Atobe, *RSC Adv.*, 2014, **4**, 57608–57610.
42 H. L. Chen, X. Jin, Y. Li and J. Tian, *RSC Adv.*, 2016, **6**, 91060–91067.

43 M. Porras, C. Solans, C. González and J. M. Gutiérrez, *Colloids Surf., A*, 2008, **324**, 181–188.
44 T. Tadros, P. Izquierdo, J. Esquena and C. Solans, *Adv. Colloid Interface Sci.*, 2004, **108–109**, 303–318.
45 Y. Ding, Q. Lin and J. Kan, *Colloids Surf., B*, 2018, **171**, 656–667.
46 S. M. Jafari, Y. He and B. Bhandari, *J. Food Eng.*, 2007, **82**, 478–488.
47 W. Li, H. Chen, Z. He, C. Han, S. Liu and Y. Li, *LWT–Food Sci. Technol.*, 2015, **62**, 39–47.
48 V. Ryu, D. J. McClements, M. G. Corradini, J. S. H. Yang and L. McLandsborough, *Food Hydrocolloids*, 2018, **82**, 442–450.
49 P. Bejrapha, M. J. Choi, S. Surassmo, J. Y. Chun and S. G. Min, *Korean J. Food Sci. Anim. Resour.*, 2011, **31**, 543–550.
50 B. Das, D. Mandal, S. K. Dash, S. Chattopadhyay, S. Tripathy, D. P. Dolai, S. K. Dey and S. Roy, *Infect. Dis.*, 2016, **9**, 11–19.
51 H. Sun, G. Li, X. Nie, H. Shi, P.-K. Wong, H. Zhao and T. An, *Environ. Sci. Technol.*, 2014, **48**, 9412–9419.
52 J. Ju, Y. Xie, H. Yu, Y. Guo, Y. Cheng, R. Zhang and W. Yao, *Food Chem.*, 2020, **310**, 125974.
53 D. B. Niu, Q. Y. Wang, E. F. Ren, X. A. Zeng, L. H. Wang, T. F. He, Q. H. Wen and C. S. Brennan, *Food Control*, 2019, **106**, 7.